

The effect of the Solar motion on the flux of long-period comets

E. Gardner^{1*}, P. Nurmi¹, C. Flynn² and S. Mikkola¹

¹*Tuorla Observatory, Department of Physics and Astronomy, University of Turku, Väisäläntie 20, FI-21500, Piikkiö, Finland*

²*Finnish Centre for Astronomy with ESO (FINCA), University of Turku, Väisäläntie 20, FI-21500, Piikkiö, Finland*

Accepted 2010 September 16. Received 2010 September 16; in original form 2010 June 24

ABSTRACT

The long-term dynamics of Oort cloud comets are studied under the influence of both the radial and the vertical components of the Galactic tidal field. Sporadic dynamical perturbation processes are ignored, such as passing stars, since we aim to study the influence of just the axisymmetric Galactic tidal field on the cometary motion and how it changes in time. We use a model of the Galaxy with a disc, bulge and dark halo, and a local disc density, and disc scale length constrained to fit the best available observational constraints. By integrating a few million of cometary orbits over 1 Gyr, we calculate the time variable flux of Oort cloud comets that enter the inner Solar System, for the cases of a constant Galactic tidal field, and a realistically varying tidal field which is a function of the Sun's orbit. The applied method calculates the evolution of the comets by using first-order averaged mean elements. We find that the periodicity in the cometary flux is complicated and quasi-periodic. The amplitude of the variations in the flux are of order 30 %. The radial motion of the Sun is the chief cause of this behaviour, and should be taken into account when the Galactic influence on the Oort cloud comets is studied.

Key words: methods: numerical – celestial mechanics – comets: general – Solar system : general – stars: kinematics and dynamics.

1 INTRODUCTION

Strong observational evidence supports the idea that the inner Solar system is subject to a steady flux of ‘new’ comets which originate from the ‘Oort cloud’ (Oort 1950). The semi-major axes of these comets are thought to evolve under the influence of external forces such as the Galactic tidal field and passing stars. The comets evolve from a typical $a_{\text{orig}} \simeq 3 \times 10^4$ AU to either hyperbolic orbits or to larger binding energies, depending on the orbital evolution during the cometary encounters with the Solar System planets. During one orbital evolution, comets typically experience perturbations that change the comet's orbit into a short-period or hyperbolic orbit, which leads to a subsequent ejection into interstellar space (Nurmi 2001).

The Galactic potential exerts a force on Oort cloud comets, and is important for the steady state flux of comets with $a > 20000$ AU, e.g. Byl (1983); Heisler & Tremaine (1986); Matese & Whitman (1989). The Galactic tidal force has a dominant component that is perpendicular to the Galactic plane; the radial component is 10 times weaker than the perpendicular component Heisler & Tremaine

(1986). For this reason, many studies (e.g. Matese et al. 1995; Wickramasinghe & Napier 2008) have assumed that the radial Galactic tidal field component is negligible. Other studies have included the radial component, for more accurate modelling of cometary motion, such as in Matese & Whitmire (1996); Brassier (2001). The radial component of the tide has been found to have an effect on the long-term evolution of the comets' perihelia, on the distribution of the longitudes of the perihelion (Matese & Whitmire 1996), and the origin of chaos in the cometary motion (Breiter et al. 2008). In recent large scale simulations, Rickman et al. (2008) found that a fundamental role is played by perturbations due to passing stars on comets, contrary to the investigations during the previous two decades, starting with Heisler & Tremaine (1986). The stellar perturbations, do of course act together with the Galactic tide.

The topic of this paper is the effect on comets due to the Galactic tide alone. We use a realistic model of the local Galaxy, which is well constrained by observations, which contains a disc, bulge and halo. We follow the orbit of the Sun in this model using recent constraints on the Solar motion. This motion allows us to compute the change in the vertical and radial components of the Galactic tide with time,

* E-mail: esgard@utu.fi

and the change in the tidal force due to the radial motion of the Sun is fully accounted for.

Qualitatively, the tidal effect on the cometary orbits can be evaluated by studying the change in angular momentum averaged over one orbit. The Galactic tidal force periodically changes the angular momentum ($J = \sqrt{GM_\odot a(1-e^2)}$) of the Oort cloud comets (Fernández & Ip 1991). The angular momentum of the comets changes as (Heisler & Tremaine 1986):

$$\frac{dJ}{dt} = -\frac{5\pi\rho_0}{GM_\odot^2} L^2 (L^2 - J^2) [1 - (J_z^2/J^2)] \sin 2\omega_g. \quad (1)$$

Here, ω_g is the Galactic argument of perihelion, J_z is the z -component of angular momentum, and is perpendicular to the Galactic plane, $L = \sqrt{\mu a}$, ρ_0 is the local mass density, and G is the gravitational constant. Note that this equation is valid for first order mean elements under the action of axially symmetric disc tides. The periodically changing angular momentum causes variations mainly in perihelion distance q , for comets in near-parabolic orbits, since $q \approx J^2/(2GM_\odot)$. The typical assumptions in the cometary flux calculations due to the Galactic tidal force suppose that the local tidal field is axisymmetric, perpendicular to the mid-plane, and adiabatically changing (Matese & Whitman 1992).

The aim of many of these studies is to correlate the motion of the Sun in the Galaxy with phenomena on the Earth, such as mass extinctions of species, the cratering record and climate change. An extensive review of this topic has been made recently by Bailer-Jones (2009).

For example, early studies have shown that the ages of well dated impact craters on Earth are not distributed randomly, but that there is a possible 28 Myr (Alvarez & Muller 1984) or 30 ± 1 Myr periodicity in crater ages over the past 250 Myr (Rampino & Stothers 1984). Since then, several authors have claimed that there is a significant periodic signal present, but the periods differ quite a lot from study to study. The signal is the most prominent for 40 large, well-dated craters that are up to 250 Myr old (Napier 2006), but the period is difficult to measure, with estimates of between 24-26 Myr (Napier 2006), 30 Myr (Napier 2006; Stothers 2006), 36 Myr (Napier 2006; Stothers 2006), 38 Myr (Yabushita 2004; Wickramasinghe & Napier 2008) and 42 Myr (Napier 2006).

In some studies, the reliability of the signal is questioned altogether, based on the inaccuracy of the age estimates of the impact craters, possible biases caused by rounding the ages of craters, and the small number of craters (Grieve & Pesonen 1996; Jetsu & Pelt 2000).

By critically reviewing many studies that have tried to connect the Solar motion and periodicity in terrestrial phenomena such as biodiversity, impact cratering and climate change, Bailer-Jones (2009) has concluded that there is little evidence to support these connections. By studying the artificial cratering data Lyytinen et al. (2009) came to the same conclusion, that the reliable detection of any periodicity is currently impossible with the existing cratering data.

In this study, we statistically analyse how the Galactic tidal force changes cometary orbits over 1 Gyr, using numerical simulations. The 1 Gyr time-scale is long enough to observe changes in the Galactic tide due to both the radial and vertical motion of the Sun. A simple axisymmetric Galactic potential is adopted. To our knowledge, there has

been no study to date, in which the effect of both radial and vertical components, in a time varying Galactic potential (via the variation in mass density ρ), has been analysed in detail. Our purpose is to study the statistical effects of the complete Galactic potential to the Oort cloud comets in detail, especially concentrating on the comets that enter the Solar System ($q < 30$ AU). In particular, we analyse the differences in cometary motion for when the tidal field is constant, and when it varies as the Sun moves in a realistic orbit in a fairly realistic Galactic potential. We find that it is important to include the radial motion of the Sun in the calculations, since the local density varies significantly as the Sun moves towards and away from the Galactic centre.

2 METHODS

The method of simulation requires two, traditionally separate, components. The first is to simulate the motion of the Sun around the Galaxy. The second involves the evolution of the orbits of comets in the Oort cloud. We integrate the motion of the Sun in an axisymmetric Galactic potential. The method of integration of the comets is described in Mikkola & Nurmi (2006). The method calculates the evolution of the comets by using first-order averaged mean elements. We do not include the random perturbations caused by the planets, since the aim is to identify the tidal effects of the Galactic potential on the flux of comets reaching the inner Solar System.

2.1 The Galactic potential

The Galactic potential consists of a disc, bulge, and dark halo, and is partially described in Gardner & Flynn (2010). The model used here differs most notably from Gardner & Flynn (2010) in the treatment of the disc, as well as a slightly modified dark halo. We noticed that the vertical density profile of the disc, from Gardner & Flynn (2010), does not accurately reproduce the observational profile from Holmberg & Flynn (2004). We proceeded to modify our disc-model by changing a few of the model's parameters, and adding three more Miyamoto-Nagai potentials to the model, to emulate a very thin layer of gas in the disc. The equation for the full potential is:

$$\Phi = \Phi_H + \Phi_C + \Phi_D + \Phi_g, \quad (2)$$

$$\Phi_H = \frac{1}{2} V_h^2 \ln(r^2 + r_0^2), \quad (3)$$

$$\Phi_C = -\frac{GM_{C1}}{\sqrt{r^2 + r_{C1}^2}} - \frac{GM_{C2}}{\sqrt{r^2 + r_{C2}^2}}, \quad (4)$$

$$\Phi_D = \sum_{i=1}^3 \frac{-GM_{d_i}}{\sqrt{(R^2 + (a_{d_i} + \sqrt{(z^2 + b^2))^2})^2}}, \quad (5)$$

$$\Phi_g = \sum_{n=1}^3 \frac{-GM_{g_n}}{\sqrt{R^2 + [a_{d_n} + \sqrt{(z^2 + b_g^2)]^2}}, \quad (6)$$

where G is the gravitational constant, R is the Galactocentric radius, and z is the height. The modified parameters are in Table 1. The vertical density profile of the model can be seen in Fig. 2.

Table 1. Parameters of the full potential.

Property	value	Unit
V_h	220	km s^{-1}
r_0	10	kpc
b	0.45	kpc
b_g	0.12	kpc
r_{C1}	2.7	kpc
r_{C2}	0.42	kpc
a_{d1}	5.81	kpc
a_{d2}	17.43	kpc
a_{d3}	34.86	kpc
M_{C1}	3	$10^9 M_\odot$
M_{C2}	16	$10^9 M_\odot$
M_{d1}	66.06×10^9	M_\odot
M_{d2}	-59.05×10^9	M_\odot
M_{d3}	22.97×10^9	M_\odot
M_{g1}	18.63×10^9	M_\odot
M_{g2}	-16.66×10^9	M_\odot
M_{g3}	6.48×10^9	M_\odot

The mass density at the Sun is $0.11 M_\odot/\text{pc}^3$, consistent with observational constraints ($0.10 \pm 0.01 M_\odot/\text{pc}^3$ Holmberg & Flynn (2000) and $0.105 \pm 0.005 M_\odot/\text{pc}^3$ Korchagin et al. (2003)). This corresponds to a nominal $T_z = 83 \times 10^6$ year period for small amplitude simple harmonic motion in the vertical direction. The surface density of disc matter in the model is $54.9 M_\odot/\text{pc}^2$, compared with a measured disc surface density of $56 \pm 6 M_\odot/\text{pc}^2$ Holmberg & Flynn (2004). The adopted current position of the Sun in the model, $(R, z)_\odot$, is (8,0) kpc. The local circular velocity of the model is 221 km s^{-1} .

2.1.1 Density and rotation curve

Fig. 1 shows the surface density of the disc with radius (R), the change in density with height (z) at the Sun ($R = 8 \text{ kpc}$) (Fig. 2), and the rotation curve (Fig. 3), as these are the two factors that have the most impact on the orbits of the comets. The disc has a scale-length of 3 kpc, and a local scale-height of 0.24 kpc, consistent with recent measurements by Jurić et al. (2008) using the Sloan Digital Sky Survey (SDSS).

The potential is axisymmetric, so we do not model effects such as molecular clouds, spiral arms, and bubbles in the interstellar matter and passing stars. Our interest here is on the global Galactic effects of the Solar motion on the comets.

2.1.2 Motion of the Sun

The orbit of the Sun, using the Solar motion measured by Schönrich et al. (2010), where $(U, V, W) = (11.1, 12.24, 7.25) \text{ km s}^{-1}$, and assuming $(R, z)_\odot$ to be (8,0) kpc, is shown in the (R, z) -plane in Fig. 4. U is the velocity towards the Galactic centre, V is the velocity along rotational direction, and W is the velocity perpendicular to the Galactic plane. Properties of this orbit, such as eccentricity, radial and vertical period and maximum z height, are shown in Table 2. The eccentricity of the Solar orbit (e) is defined as: $(R_{\text{max}} - R_{\text{min}})/(R_{\text{max}} + R_{\text{min}})$.

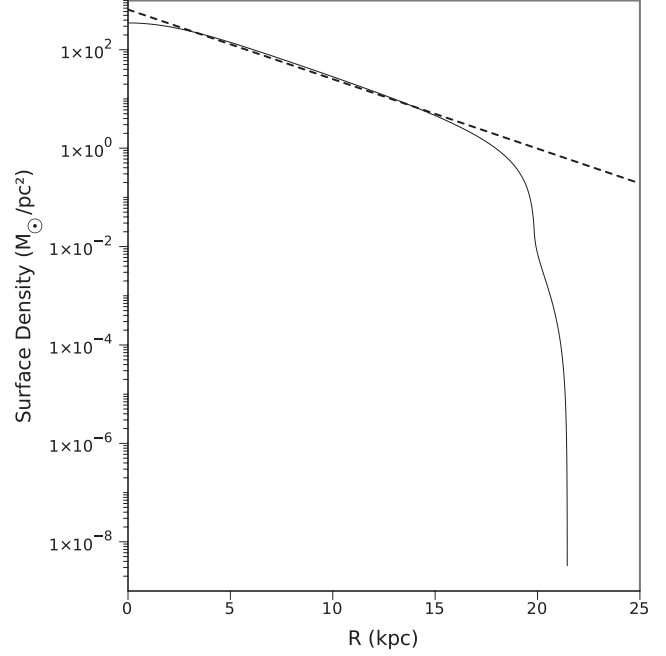


Figure 1. The surface density of the disc component as a function of Galactocentric radius. The dashed line corresponds to an exponential density falloff of 3 kpc, which is a good fit to the model over a wide range of radii. Note that the density truncates strongly at 18 kpc.

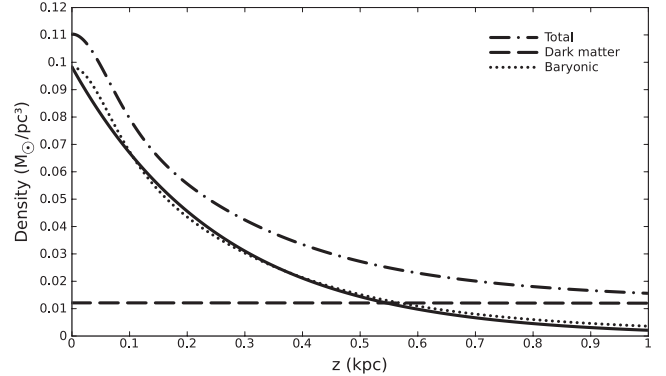


Figure 2. Vertical density of the model, at the Sun ($R = 8 \text{ kpc}$). The dotted line represents the baryonic contribution in the model, the dashed line the dark matter contribution, and the dashed-dotted line the total density of the model at a certain height (z). The solid line corresponds to an exponential fit to the baryonic component of the model of 0.25 kpc.

Table 2. Eccentricity, e , maximum vertical height, z_{max} , radial oscillation period, T_R , and vertical oscillation period, T_z , of the Sun in the adopted potential. The adopted solar motion is that of Schönrich et al. (2010).

Property	value	Unit
e	0.059 ± 0.003	
z_{max}	0.102 ± 0.006	kpc
T_R	149 ± 1	Myr
T_z	85 ± 4	Myr

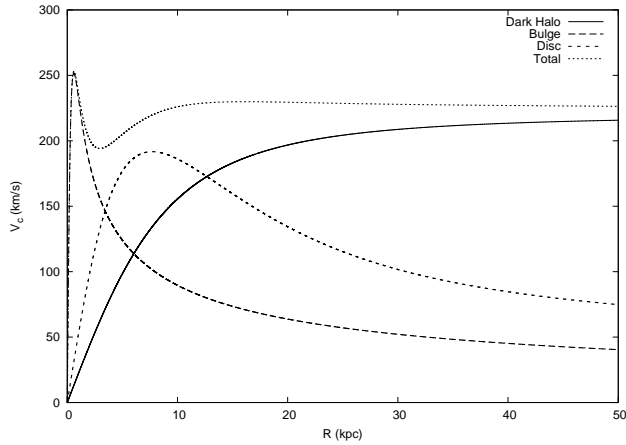


Figure 3. Rotation curve for the model Milky Way (dotted), and the different contributions of the disc (dashed), bulge (long dashed), and dark halo (solid).

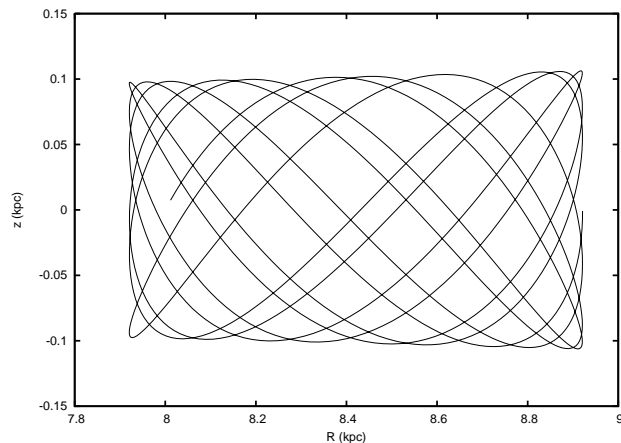


Figure 4. Motion of the Sun in the model potential for 1 Gyr, in radial R and vertical z components. The initial position of the Sun is $(R, z)_0 = (8, 0)$ kpc.

2.2 Variation of the tidal parameters caused by the motion of the Sun

Our integration method for cometary motion is based on the computation of secular motion of the comet in quadratic perturbation by the Galactic potential. The method used is presented in Mikkola & Nurmi (2006). As the comet orbits the Sun under the Galactic potential it experiences a force \mathbf{F} per unit mass:

$$\mathbf{F} = -\frac{GM_\odot}{r^3}\mathbf{r} - G_1x\mathbf{x} - G_2y\mathbf{y} - G_3z\mathbf{z}, \quad (7)$$

where $G_1 = -(A - B)(3A + B)$, $G_2 = (A - B)^2$, and $G_3 = 4\pi G\rho(R, z) - 2(B^2 - A^2)$. Here r is the Sun-Comet distance, $\rho(R, z)$ is the local mass density, and G is the gravitational constant (Heisler & Tremaine 1986). A and B are the Oort constants, and are obtained from the Galactic model. Usually the radial components (x, y) are neglected, so that $G_1 = G_2 = 0$.

We will examine the effect on comets in two particular cases. Firstly we study what we call the 'dynamic' case, in which the Galactic tide changes realistically along the Solar orbit, for the case that the Sun oscillates both vertically and

radially in the potential. Secondly, we assume that there is a 'constant' tidal field (i.e. the tidal field does not change as the Sun moves around the Galaxy). In the constant case the Sun moves on a flat, circular orbit.

We integrate the Solar orbit in the 'dynamic' case for 1 Gyr, sampling the values of the G -parameters every 100 kyr: these are shown in Fig. 5. The changes in G_3 are dominated by the changes in local density during the orbit, since the changes in A and B over the orbit are not very large. Fig. 5 (top and centre panel) shows how the changing values of the Oort constants, A and B , affect the values of G_1 and G_2 .

Fig. 6 shows the combined effects of the radial (R) and vertical motion (z) of the orbit, on G_3 . It is clear that G_3 increases in two situations: when the radial position is the closest to the Galactic centre, and when the vertical motion crosses the mid-plane. Due to the slightly eccentric motion of the orbit, it is the radial component of the motion which dominates the changes in local density ($\rho(R, z)$), rather than the vertical motion. This is partly because we adopt the Solar motions of Schönrich et al. (2010), which produces a mildly eccentric orbit for the Sun ($e = 0.059 \pm 0.003$): it oscillates between Galactocentric radii of 7.9 and 8.9 kpc. As such, the evolution of G_3 depends on the radial motion and the vertical motion, both being of equal magnitude (Fig. 6).

In the second case studied, the Sun is set on a perfectly circular and flat orbit, so that the local mass density does not change with time. For the 'constant' case, the values of G_i are the mean values from the 'dynamical' case, and have the values $G_1 = -7.00897 \times 10^{-16}$, $G_2 = 7.27613 \times 10^{-16}$, and $G_3 = 4.55749 \times 10^{-15} \text{yr}^{-2}$.

3 SIMULATIONS OF THE COMETS

Observations support the idea that the *in situ* flux of new comets is roughly linear with respect to heliocentric distance, up to the distance of Jupiter (Hughes 2001). Comets with highly eccentric orbits with randomised directions of motion have a q -distribution that is flat (Öpik 1966). If a long period comet has a perihelion distance between ~ 10 – 15 AU, it is quickly ejected to interstellar space or perturbed so that it becomes a short-period comet (Wiegert & Tremaine 1999). From the perspective of the Oort cloud, the comets are removed from the Oort cloud and from the loss cone to the orbital parameter distribution (Fernández 1981). The loss cone (lc) is the population of comets that have orbits that will allow them to penetrate the planetary system, making it possible to observe them (Hills 1981). Planetary perturbations move comets efficiently from q values less than $q_{lc} \simeq 15$ AU into either hyperbolic orbits or into orbits that are more tightly bound to the solar system (Hills 1981). In the steady state situation, the new comets are distributed uniformly to the perihelion distances of $q \leq q_{lc}$, for $a > 30000$ AU, while $q > q_{lc}$ comets come also from the inner region. For this reason, in all of our simulations we have assumed that initial perihelion distances are distributed uniformly outside the loss cone. The inclination distribution of the outer Oort cloud of comets is isotropic (uniform in $\cos i$). All the other angular elements are uniformly distributed between $[0 - 2\pi]$.

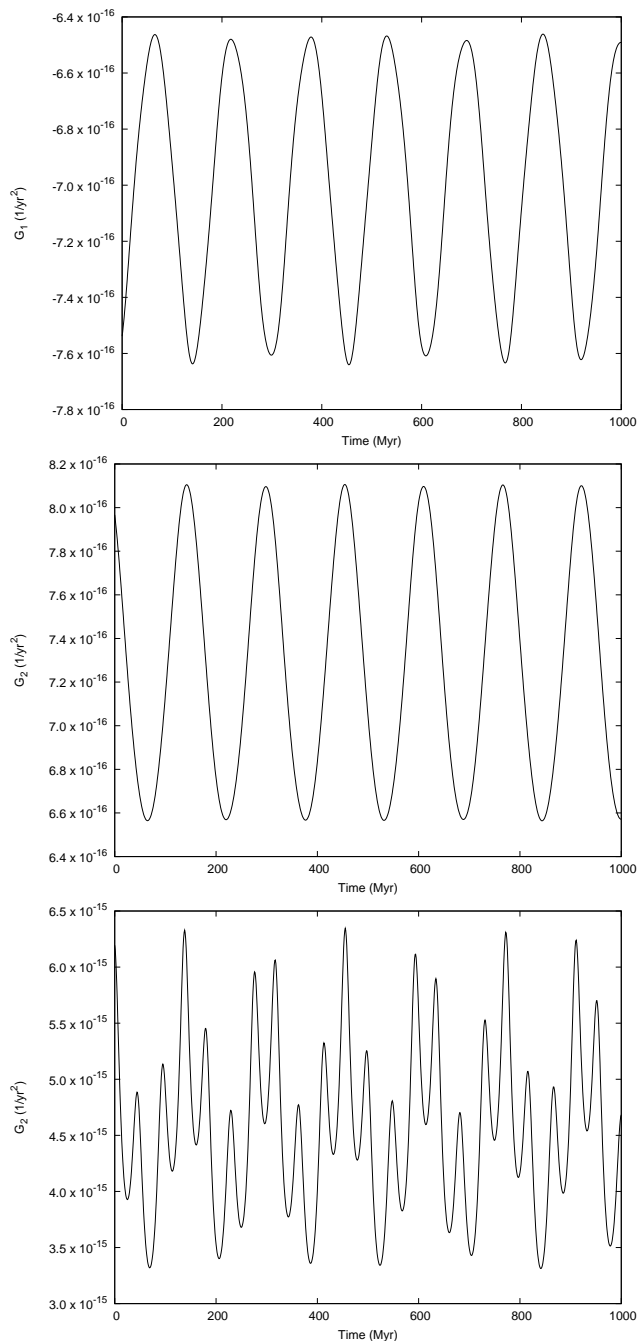


Figure 5. Variation of the parameters G_1 (top panel), G_2 (centre panel), and G_3 (bottom panel) along the Solar orbit in the ‘dynamic’ case (i.e. including full vertical and radial motions) over 1 Gyr.

3.1 Structure of the Oort cloud

An important issue in studying the structure of the Oort cloud, is what energy distribution to adopt for the comets. We assume that the density of comets between 3000 AU and 50000 AU in the Oort cloud is proportional to $1/r^{3.5 \pm 0.5}$, so that the number of comets N is $dN \propto 1/r^\alpha dr$, where $\alpha = 1.5 \pm 0.5$ (Duncan et al. 1987). The conclusions of this paper are not particularly sensitive to the adopted value of α . The existence of an inner Oort cloud has been speculated upon in many studies although there is no direct evidence for

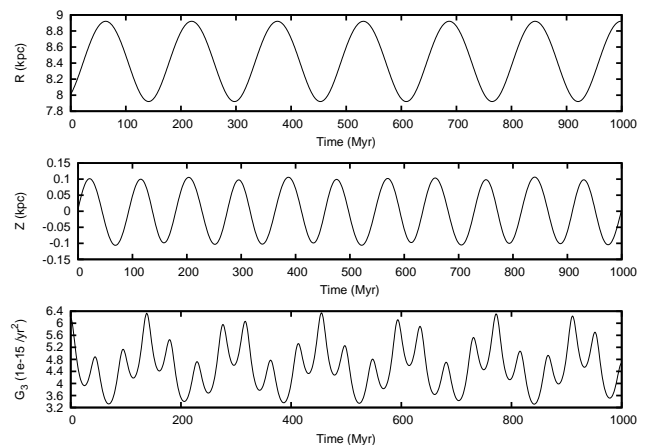


Figure 6. Galactocentric radius R , vertical height z and G_3 for the ‘dynamic’ case of the Solar motion over 1 Gyr in the Galactic adopted model. Upper panel: the radial motion. Middle panel: vertical motion. Lower panel: G_3 .

it (Hills 1981). An inner Oort cloud is the extension of the Kuiper belt, filling the gap between the Kuiper belt and the outer Oort cloud. Semi-major axes in the inner Oort cloud are typically between 50–15000 AU (Leto et al. 2008). The steady state flux from the inner Oort cloud cannot be uniformly distributed in perihelion distance, since the planetary perturbations move comets efficiently from q values less than $q_{lc} \simeq 15$ AU to either hyperbolic orbits or into orbits that are more tightly bound to the solar system (Hills 1981). In the steady state situation, the new comets come uniformly to perihelion distances $q \leq q_{lc}$ when $a > 30000$ AU, while the $q > q_{lc}$ comets also come from the inner region.

3.2 Simulation parameters of the comets

Due to this complicated picture, we study different semi-major axes in separate simulations, and evaluate the efficiency of tidal injection in each simulation. We chose initial sample conditions for the Oort cloud comets, setting the semi-major axis to be 10000, 20000, 30000, 40000, 50000, and 60000 AU. We choose the comet’s eccentricity (e) randomly, so that the resulting values of q would be uniformly distributed from 35 to the value of the semi-major axis (a). All the other parameters, $\cos(i)$, Ω , ω , and the initial eccentric anomaly were all chosen randomly in appropriate intervals. The number of comets in each simulation is 10^6 at each of the sampled semi-major axes. For the computation of the numbers of comets reaching the inner Solar System, the results from each semi-major axis are normalised to the adopted number density law.

3.3 Simulations of the Galactic tide

To study the effect of the Galactic potential on cometary motion, we chose two hypothetical solar systems: a ‘constant’ background density, where the Sun would be on a pure circular orbit with no vertical motion, and a realistic ‘dynamic’ Solar orbit. In all systems, we analyse the flux of Oort cloud comets into the Solar System. This means that we consider a comet to have been detected in the inner Solar System when its q is within 30 AU, and it has

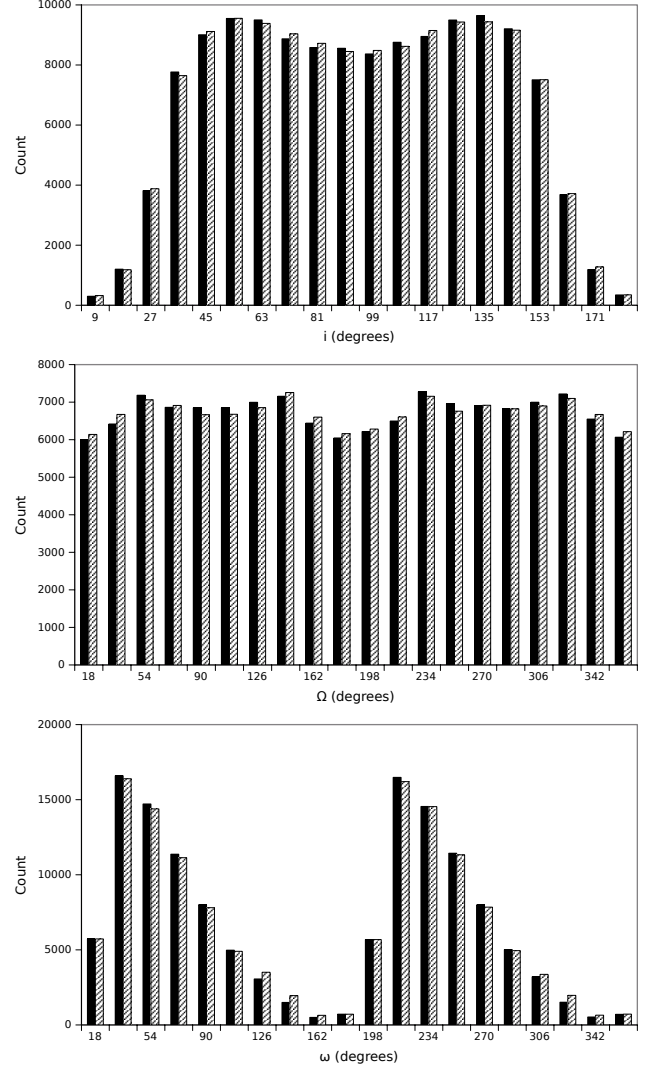
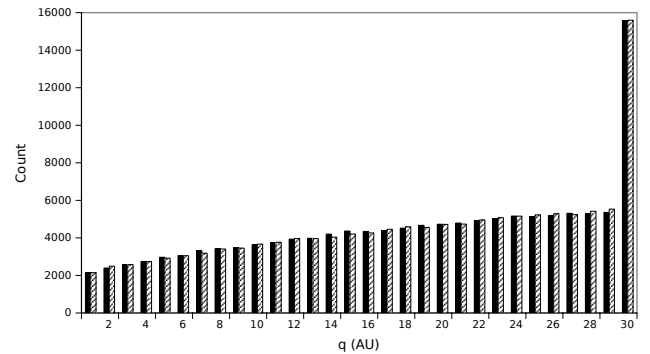
Table 3. Relative fraction of comets entering the inner Solar System, from each of the simulated semi-major axis values, for the ‘constant’ and ‘dynamic’ cases.

Semi-major axis (AU)	constant	dynamic
10000	0.0729	0.0732
20000	0.1803	0.1804
30000	0.2405	0.2405
40000	0.2381	0.2369
50000	0.1504	0.1507
60000	0.1179	0.1184

a heliocentric radius of less than 1000 AU. The last criterion is important, as the osculating elements of comets can evolve to have $q \leq 30$ AU, far away from the Sun, and evolve to more than 30 AU, without ever entering the inner Solar System. Since the minimum of the osculating q is at the aphelion, the criterion $q \leq 30$ AU is approximate. For this reason, we also check if the comet is actually approaching the aphelion, by choosing $r < 1000$ AU. This requires use of the mean anomaly, which is approximately calculated from the derived time co-ordinate. Comets which have been detected are removed from the simulation. We do not replace them with new comets.

4 RESULTS

Our aim is to determine the effect of the Galactic tide on Oort cloud comets by separately adopting a constant local density and a varying local density. Examining the flux of comets into the inner Solar System (Table 3), we find that there is no significant difference between the two models. Most of the detected comets come from the middle (30–40 kAU) range of semi-major axes. Likewise, the resulting distribution of orbital elements, for comets coming into the Solar System, is the same in both the constant and dynamic cases. Fig. 7 shows example distributions for the simulation cases where the semi-major axis is 30000 AU. The gap at $\omega = 0$ and 180 is caused by the $\sin 2\omega_g$ term going to 0 in Equation 1. Similarly, the factor $1 - (J_z^2/J^2)$ goes to zero at $i=0$ or 180, since $J_z = J \cos i$. The q -distribution of incoming comets shows no significant difference between the two cases, as seen in Fig. 8. The high peak at $q = 30$ AU, in Fig. 8 is caused by the slow evolution of q , at $a = 30000$ AU. Finally, the total flux of comets entering the inner-Solar system is not significantly different between the two cases. For the ‘constant’ case, from a source pool of 1.8 million comets in the simulated Oort cloud, we find that approximately 120 comets per Myr reach the inner Solar System (which here means comets with $q < 30$ AU). Assuming that there are about 10^{12} comets in the Oort cloud (Wiegert & Tremaine 1999), this corresponds to about 70 comets per year with $q < 30$ AU. This is a bit higher than the observed number of new comets with $q < 30$ AU, which is about 20 per year, assuming a cometary flux of $0.65 \pm 0.18 \text{ yr}^{-1} \text{ AU}^{-1}$ (Fernández 2010).

**Figure 7.** Distribution of the orbital elements i , Ω , and ω for $a = 30000$. The solid column represents constant case, and the shaded column the dynamic case. There is no significant difference between the two distributions.**Figure 8.** Distribution of the perihelion distance q for the incoming comets, for $a = 30000$. The solid column represents the constant case, and the shaded column the dynamic case. There is no significant difference between the two distributions.

4.1 Time evolution of the cometary flux

There is a clear difference between the two models when we look at the temporal evolution of the cometary flux. The top panel of Fig. 9 shows, for the 'dynamic' case (and after a relaxation time of about 100 Myr) that the mean cometary flux (shown as a 10 Myr moving average) is well correlated with the changes in G_3 (dashed line). The resulting fluxes from the simulation have been weighted according to their relative number-density ($a^{-1.5}$), the resulting total amount of comets in the simulation, by using this weighting system is 1.8×10^6 . From Section 2.2, there are two main causes for the evolution of the flux, the major being the radial motion, the minor being the vertical motion. The top panel of Fig 9 shows the major trend clearly following the radial motion. The vertical motion is also followed, as is clear in the 10 Myr moving average (which smooths out some of the Poisson noise in the individual 1 Myr samples). We also ran a separate simulation with a circular orbit, and with the vertical component intact, the resulting fluxes followed perfectly the vertical motion, as was expected due to the changes in G_3 being solely contributed by the vertical component. In the case where the values for G_i have been kept constant (i.e. corresponding to a completely circular orbit with no vertical motion), there is no evidence of any evolution, as seen in the bottom panel of Fig. 9.

Simple Fourier-analysis of the dynamic flux (in the top panel of Fig. 9) finds two distinct periods in the cometary flux. The strongest signal is produced by a period of 143–167 Myr, and an equal signal from a period of 41–45 Myr. The former corresponds to the radial period (152 Myr) and the latter to the half-period of the vertical period (43 Myr). The vertical signal is found to lie in the range 41–45 Myr, and is quasi-periodic, as has been seen earlier by Matese et al. (2001).

4.2 Comparison with earlier results

Matese et al. (1995) derived various periods for the vertical Solar oscillation, depending on the adopted model of the disc. For example, their 'No-Dark-Disk Model' has a crossing-period very close to ours (43 Myr), while their 'Best-fit Model' produces a much lower period of 33 Myr. They assumed a W -velocity of 7.5 km s^{-1} , compared to ours of 7.25 km s^{-1} , and does not cause much qualitative difference in the vertical period of the orbit of the Sun. The lower period comes from assuming a considerably higher mid-plane density ($\rho \approx 0.13 \text{ M}_\odot/\text{pc}^3$) than ours.

Matese et al. (2001) found that the radial period of Solar motion modulates the vertical period. However, they used very high local densities of matter in the disc, so that the vertical oscillations dominated the radial oscillations. This meant that the flux of comets into the inner Solar System with each passage through the disc was greatly amplified compared to our simulations. We find that the cometary flux varies with an amplitude of about 20%, whereas Matese et al. (2001) find flux variations of about a factor of two. The much smaller amplitude in the signal which we advocate, even taking into account the radial oscillations, would make finding a period in the scant cratering record very difficult.

Fouchard et al. (2006) calculated that a local mass den-

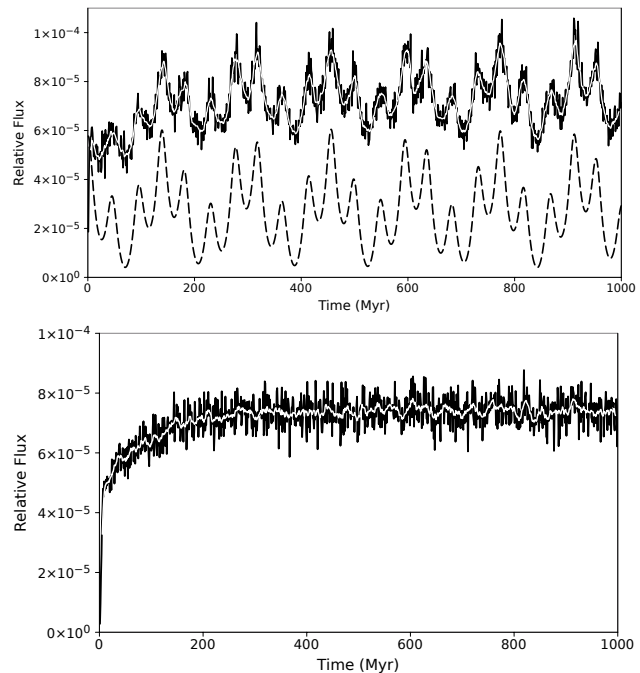


Figure 9. The time evolution of the relative flux of comets in the dynamic case (top panel), and the constant case (bottom panel). The solid line represents the relative flux of comets in 1 Myr bins, the white line a 10 Myr moving average. The dashed line in the top panel represents the evolution of the G_3 -parameter.

sity of $\rho = 0.1 \text{ M}_\odot/\text{pc}^3$ corresponds to a cometary flux of around 10^4 for their first 500 Myr interval for a source population of 10^6 comets, where observed comets have $q \leq 15 \text{ AU}$. Assuming that there are 10^{12} comets in the Oort cloud. This produces a flux of ~ 20 comets/yr, which is a factor of two less than our estimate.

The Galactic tide case in Rickman et al. (2008) gives a flux of 100 comets per 50 Myr, from a source population of 10^6 comets, where observed comets have evolved from $q > 15 \text{ AU}$ to $q < 5 \text{ AU}$. This corresponds to a flux of 2 comets/yr, again assuming an Oort cloud with 10^{12} comets. Using similar analysis we find that we get a flux of 290 comets per 50 Myr, corresponding to a factor of three larger than Rickman et al. (2008).

A review by Bailer-Jones (2009) correlates terrestrial events with cometary signals. One of the more interesting ones in the review is the $140 \pm 15 \text{ Myr}$ period found by Rohde & Muller (2005) in the number of known marine animal genera as a function of time. While this could correspond to the Sun's radial period, Bailer-Jones (2009) considers that it has not been significantly detected, the main problem being that the entire time-span of the data covers no more than three oscillations. Many other periods, proxies, and studies are mentioned in Bailer-Jones (2009), although the conclusion is that there is no proven impact on biodiversity as a result of the orbital motion of the Sun.

5 DISCUSSION AND CONCLUSIONS

We have studied the long-term dynamics of Oort cloud comets under the influence of both the radial and the ver-

tical components of the Galactic tidal field. Other perturbing forces on the comets, such as passing stars or passage through spiral arms are ignored, since we aim to study the influence of just the axisymmetric Galactic tidal field on the cometary motion.

We use an axisymmetric model of the Galaxy, and a recently revised value for the Solar motion by Schönrich et al. (2010). This leads to vertical oscillations of the Sun with an amplitude of about 100 pc, and radial oscillations over about 1 kpc. The changing tidal forces on the Oort cloud are computed as the Sun orbits for 1 Gyr in this potential, and the flux of comets entering the inner Solar System is computed in simulations.

As expected, the cometary flux is strongly coupled to the G_3 -parameter in the tidal forces, which is dominated by the local mass density seen along the Solar orbit. Both the radial and vertical motions of the Sun can be seen in the cometary flux, although the amplitude of the variations is small, implying that detecting such a signal from the small number of age-dated craters would be very difficult. This agrees with the recent review of the detectability of the Solar motion in terrestrial proxies (Bailer-Jones 2009).

As G_3 is directly coupled to local density, it is easily affected by the non-axisymmetric components in the motion of the Sun in the Galaxy. This implies that spiral arms, a Galactic bar, giant molecular clouds, or any other intermittently encountered structure should have an effect on the flux.

ACKNOWLEDGEMENTS

PN wants to thank the Academy of Finland for the financial support in this work. EG acknowledges the support of the Finnish Graduate School in Astronomy and Space Physics.

REFERENCES

- Alvarez W., Muller R. A., 1984, *Nature*, 308, 718
 Bailer-Jones C. A. L., 2009, *International Journal of Astrobiology*, 8, 213
 Brassier R., 2001, *MNRAS*, 324, 1109
 Breiter S., Fouchard M., Ratajczak R., 2008, *MNRAS*, 383, 200
 Byl J., 1983, *Moon and Planets*, 29, 121
 Duncan M., Quinn T., Tremaine S., 1987, *AJ*, 94, 1330
 Fernández J. A., 1981, *A&A*, 96, 26
 Fernández J. A., 2010, in J. A. Fernández, D. Lazzaro, D. Prialnik, & R. Schulz ed., *IAU Symposium Vol. 263 of IAU Symposium, The discovery rate of new comets in the age of large surveys. Trends, statistics, and an updated evaluation of the comet flux.* pp 76–80
 Fernández J. A., Ip W., 1991, in R. L. Newburn Jr., M. Neugebauer, & J. Rahe ed., *IAU Colloq. 116: Comets in the post-Halley era Vol. 167 of Astrophysics and Space Science Library, Statistical and evolutionary aspects of cometary orbits.* Kluwer Academic Publishers, Dordrecht, the Netherlands, 1991., pp 487–535
 Fouchard M., Froeschlé C., Valsecchi G., Rickman H., 2006, *Celestial Mechanics and Dynamical Astronomy*, 95, 299
 Gardner E., Flynn C., 2010, *MNRAS*, 405, 545
 Grieve R. A. F., Pesonen L. J., 1996, *Earth Moon and Planets*, 72, 357
 Heisler J., Tremaine S., 1986, *Icarus*, 65, 13
 Hills J. G., 1981, *AJ*, 86, 1730
 Holmberg J., Flynn C., 2000, *MNRAS*, 313, 209
 Holmberg J., Flynn C., 2004, *MNRAS*, 352, 440
 Hughes D. W., 2001, *MNRAS*, 326, 515
 Jetsu L., Pelt J., 2000, *A&A*, 353, 409
 Jurić M., Ivezić Ž., Brooks A., Lupton R. H., Schlegel D., et al. 2008, *ApJ*, 673, 864
 Korchagin V. I., Girard T. M., Borkova T. V., Dinescu D. I., van Altena W. F., 2003, *AJ*, 126, 2896
 Leto G., Jakubík M., Paulech T., Neslušan L., Dybczyński P. A., 2008, *MNRAS*, 391, 1350
 Lyytinen J., Jetsu L., Kajatkari P., Porceddu S., 2009, *A&A*, 499, 601
 Matese J. J., Innanen K. A., Valtonen M. J., 2001, in M. Y. Marov & H. Rickman ed., *Astrophysics and Space Science Library Vol. 261 of Astrophysics and Space Science Library, Variable Oort cloud flux due to the Galactic tide.* pp 91–102
 Matese J. J., Whitman P. G., 1989, *Icarus*, 82, 389
 Matese J. J., Whitman P. G., 1992, *Celestial Mechanics and Dynamical Astronomy*, 54, 13
 Matese J. J., Whitman P. G., Innanen K. A., Valtonen M. J., 1995, *Icarus*, 116, 255
 Matese J. J., Whitmire D., 1996, *ApJL*, 472, L41+
 Mikkola S., Nurmi P., 2006, *MNRAS*, 371, 421
 Napier W. M., 2006, *MNRAS*, 366, 977
 Nurmi P., 2001, *MNRAS*, 323, 911
 Oort J. H., 1950, *BAN*, 11, 91
 Öpik E. J., 1966, *Irish Astronomical Journal*, 7, 141
 Rampino M. R., Stothers R. B., 1984, *Nature*, 308, 709
 Rickman H., Fouchard M., Froeschlé C., Valsecchi G. B., 2008, *Celestial Mechanics and Dynamical Astronomy*, 102, 111
 Rohde R. A., Muller R. A., 2005, *Nature*, 434, 208
 Schönrich R., Binney J., Dehnen W., 2010, *MNRAS*, 403, 1829
 Stothers R. B., 2006, *MNRAS*, 365, 178
 Wickramasinghe J. T., Napier W. M., 2008, *MNRAS*, 387, 153
 Wiegert P., Tremaine S., 1999, *Icarus*, 137, 84
 Yabushita S., 2004, *MNRAS*, 355, 51